On the Spatial Instability Modes of the Laminar Ekman Boundary Layer

STUART W. MARLATT AND SEDAT BIRINGEN

Department of Aerospace Engineering, University of Colorado, Boulder, Colorado

16 April 1993 and 19 April 1994

1. Introduction

The stability of the Ekman boundary layer is of interest largely due to the observed similarity between large-scale lineal structures in the atmosphere and the roll structure of the primary instabilities of the laminar Ekman layer. Although many of the large-scale rolls in the atmospheric boundary layer are dominated by convective mechanisms, the role of shear instabilities in initiating vertical motions preceding cloud development has been suggested by several researchers, notably Faller (1965), Brown (1980), and Etling and Brown (1993).

Examination of laminar Ekman layer instability by experimental studies (see Faller 1990) and through the solution of the linearized instability equations (e.g., Melander 1983) has resulted in refined values for phase speed, orientation, and critical Reynolds numbers for two primary instabilities. The Type I instability is an inflectional instability, which grows via extraction of energy from the component of the mean flow perpendicular to the instability roll axis and appears as a nearly stationary wave with a critical Reynolds number of 112. The Type II instability is commonly termed a "parallel" instability, since it extracts energy from the component of the mean flow parallel to the roll axis, through an interaction with the Coriolis terms. The Type II instability is observed as a rapidly traveling wave with a critical Reynolds number of 54. Several studies, including those of Faller, have noted that the early onset of Type II waves may suppress development of Type I waves, leading to speculation that the Type II waves are an important path to turbulence in the laminar Ekman layer. While most studies of large-scale rolls in the atmospheric boundary layer have focused on Type I instabilities, both Type I and Type II are observed (Shirer 1986; Stensrud and Shirer 1988).

Previous linear stability studies of the Ekman layer have considered only temporal stability. The results from these studies have generally compared well with experimental results; however, experimentally observed waves tend to be more closely aligned with the geostrophic free stream than predicted by theory [Faller and Kaylor 1966; Tatro and Mollo-Christensen 1967; Caldwell and Van Atta 1970; a review of the pertinent experimental findings is given by Caldwell and Van Atta (1970)]. Since physical phenomena are observed in a spatial reference frame, consideration of spatial instability modes of the Type II instabilities should prove interesting, to identify whether the observed discrepancy is a result of the temporal approximation. This note briefly addresses this issue.

2. Relations between temporal and spatial instability modes

The Ekman layer linear stability problem is generally approached as a two-dimensional problem, utilizing a coordinate system rotated about the surface normal axis (y) by an angle ϵ (+CCW) such that the z axis is aligned with the axis of the instability (cf. Lilly 1966), allowing the linear stability equations to be written

$$\phi^{IV} - 2\alpha^2\phi'' + \alpha^4\phi - i\alpha \,\mathrm{Re}[(U - c) \times (\phi'' - \alpha^2\phi) - U''\phi] + 2\mu' = 0 \quad (1a)$$

$$\mu'' - \alpha^2\mu - i\alpha \,\mathrm{Re}[(U - c)\mu + W'\phi] - 2\phi' = 0. \quad (1b)$$

In Eqs. (1a,b) the Reynolds number is based on the geostrophic velocity V_g, the Ekman depth $\delta_E = \sqrt{\nu/\Omega}$, and the molecular kinematic viscosity ν, $\mathrm{Re} = V_g\delta_E/\nu$, where Ω is the system rotation rate. The quantities U and W are the x and z velocity components of the laminar base flow in the rotated coordinate system, and $'$ denotes differentiation with respect to y. The perturbation streamfunction $\psi \,\|\, u = -\partial\psi/\partial y$, $v = \partial\psi/\partial x$ and the spanwise velocity w take the form

$$\psi(x, y, t) = \phi(y)e^{i(\alpha x - \omega t)} \quad (2a)$$

$$w(x, y, t) = \mu(y)e^{i(\alpha x - \omega t)}. \quad (2b)$$

In general, α and c are complex, representing instabilities along a continuum between temporal modes (α real) and spatial modes (c real). The parameters α, c,

Corresponding author address: Stuart W. Marlatt, Dept. of Aerospace Engineering Sciences, University of Colorado, Boulder, CO 80309.

TABLE 1. Ekman layer primary instability modes. Comparison of the linear solver results with values graphically interpolated from Melander (1983).

Re	α	ϵ	c	c (ref)
54.15504	0.31623	−23.3261	(0.616, 5.98e − 4)	(0.616, 0.0)
65.0	0.314	−20.8	(0.572, 6.98e − 3)	(0.574, 6.85e − 3)
75.0	0.306	−18.7	(0.540, 1.15e − 2)	(0.542, 1.11e − 2)
85.0	0.300	−17.0	(0.513, 1.49e − 2)	(0.514, 1.48e − 2)
95.0	0.298	−15.6	(0.489, 1.74e − 2)	(0.489, 1.73e − 2)
100.0	0.292	−15.0	(0.482, 1.89e − 2)	(0.482, 1.88e − 2)
105.0	0.289	−14.5	(0.473, 1.98e − 2)	(0.471, 1.98e − 2)
115.0	0.287	−13.1	(0.452, 2.14e − 2)	(0.454, 2.14e − 2)
125.0	0.283	−12.0	(0.435, 2.28e − 2)	(0.439, 2.29e − 2)
150.0	0.275	−10.0	(0.402, 2.56e − 2)	(0.400, 2.56e − 2)

and $\omega = \alpha c$ have distinct physical significance: the wavenumber is given by α_r, the spatial growth rate by α_i, the phase velocity by c_r, the frequency by ω_r, and the temporal growth rate by ω_i, where the subscripts r and i indicate real and imaginary parts of the complex value, respectively. Temporal solutions are considered unstable if ψ (or w) grows with t, that is, if $\omega_i > 0$. Similarly, spatial solutions are unstable for $\alpha_i < 0$.

Typically, linear stability studies consider only the temporal modes, solving (1a,b) as a linear eigenvalue problem for c, assuming fixed values for α_r and Re. It is possible to obtain directly the spatial modes (e.g., Danabasoglu and Biringen 1990) by assuming ω_r and Re and solving the nonlinear eigenvalue problem for α. In an alternative and simpler approach, the spatial eigenvalues may be determined from a knowledge of the temporal instability modes and the group velocity $\partial\omega_r/\partial\alpha_r$.

Gaster's relations (1962) allow the spatial eigenvalues to be obtained from temporal eigenvalues, using the temporal eigenvalues to compute the group velocity. Denoting the temporal modes by (T) and the spatial modes by (S), Gaster's relations may be summarized as

$$\alpha_r(T) \approx \alpha_r(S) \tag{3a}$$

$$\omega_r(T) \approx \omega_r(S) \tag{3b}$$

$$\frac{\omega_i(T)}{\alpha_i(S)} \approx -\frac{\partial\omega_r}{\partial\alpha_r}, \tag{3c}$$

which are accurate for parallel, two-dimensional boundary layers to $O(\omega_i^2)$, under the condition that $\partial\omega_i/\partial\alpha_i$ is of the same order as the maximum temporal growth rate at the Reynolds number of interest.

As Gaster's analysis considers only the relation between α and ω, (3a,b,c) may be immediately applied to the Ekman layer to evaluate the spatial eigenvalues from the results of temporal-mode computations.

3. Discussion of results

Equations (1a,b) were solved for the eigenvalues c and eigenvectors ϕ and μ at given Re and α using a second-order finite-difference method and QZ eigenvalue solver (Van Dooren 1982). The technique was validated by comparison of eigenvalues and eigenvectors with Melander (1982); a list of eigenvalue comparisons for the Type II instability is presented in Table 1. Temporal eigenvalues were computed for Reynolds numbers of 65 and 100; group velocities were computed from the temporal data using fourth-order finite differences, and the spatial eigenvalues were computed from (3a,b,c). Figure 1 presents both temporal and spatial growth rate contours for Re = 65 and Re = 100.

The spatial evolution of small amplitude disturbances in the Ekman layer was also investigated using a three-dimensional, time-dependent, incompressible Navier–Stokes solver to numerically integrate the governing equations by a mixed spectral–finite difference method (Danabasoglu et al. 1991), as an adjunct to a related study (Marlatt and Biringen 1994). In the present simulations, prescribed time-dependent inflow velocity perturbations are allowed to grow in a spanwise periodic domain, using a nonreflective outflow boundary condition. The inflow conditions consisted of perturbation velocities derived from the eigenvectors of the linear instability equations (1a,b) and transforming the temporal eigenvalues using (3a,b,c). Note that the Gaster transformations do not affect the eigenvectors; that is, the eigenvectors for the temporal and spatial cases are identical. A comparison of the perturbation velocity contours obtained from a numerical simulation at Re = 65 and those from the linear theory is presented in Figs. 2a and 2b, showing excellent agreement. The small amplitude errors noted far from the wall, especially in the u velocity contours, arise from coarse computational grid resolution in these regions. The close agreement of the direct simulation results with the spatially evolving linear solution confirms the applicability of the Gaster relations to the Ekman layer stability problem.

4. Conclusions

Gaster's theoretical relationship between temporally and spatially evolving instability modes has been ap-

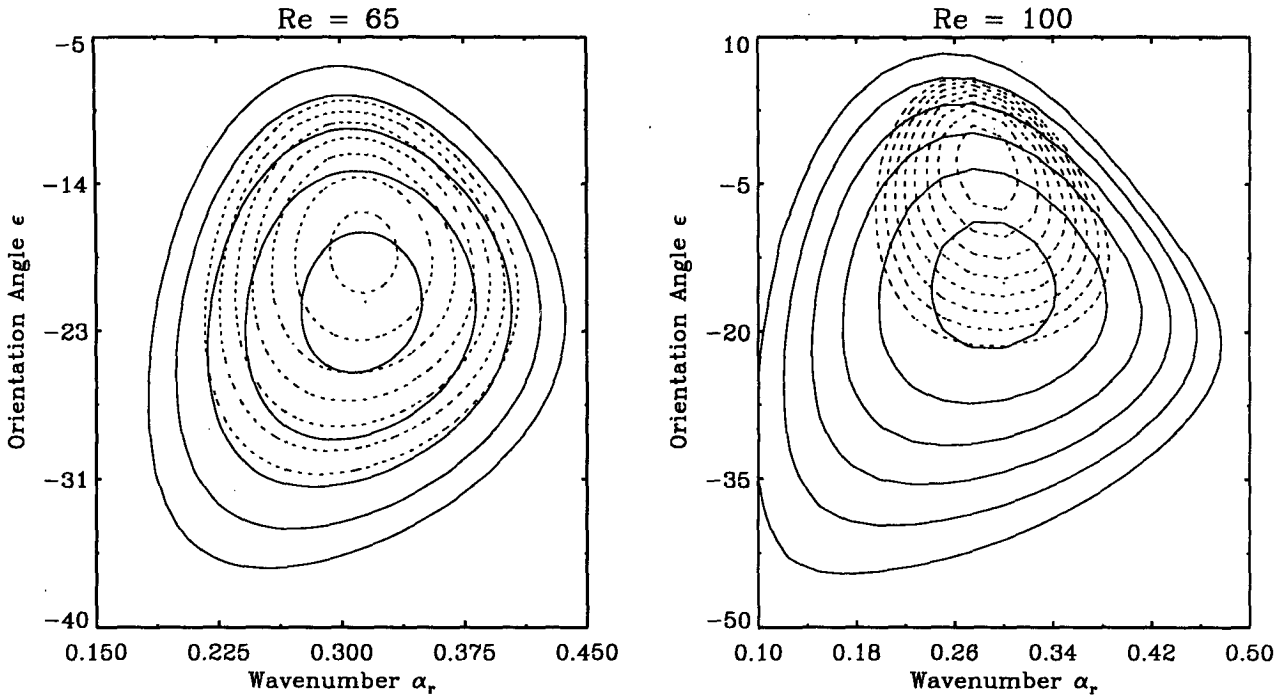

FIG. 1. Temporal (ω_i) and spatial (α_i, dotted) growth rates. (a) Re = 65. Contour interval 0.0005 for ω_i and -0.0005 for α_i; minimum contour levels 0.0 and -0.002 for ω_i and α_i, respectively. (b) Re = 100. Contour interval is 0.001 for ω_i and -0.001 for α_i; minimum contour levels 0.0 and -0.011 for ω_i and α_i, respectively.

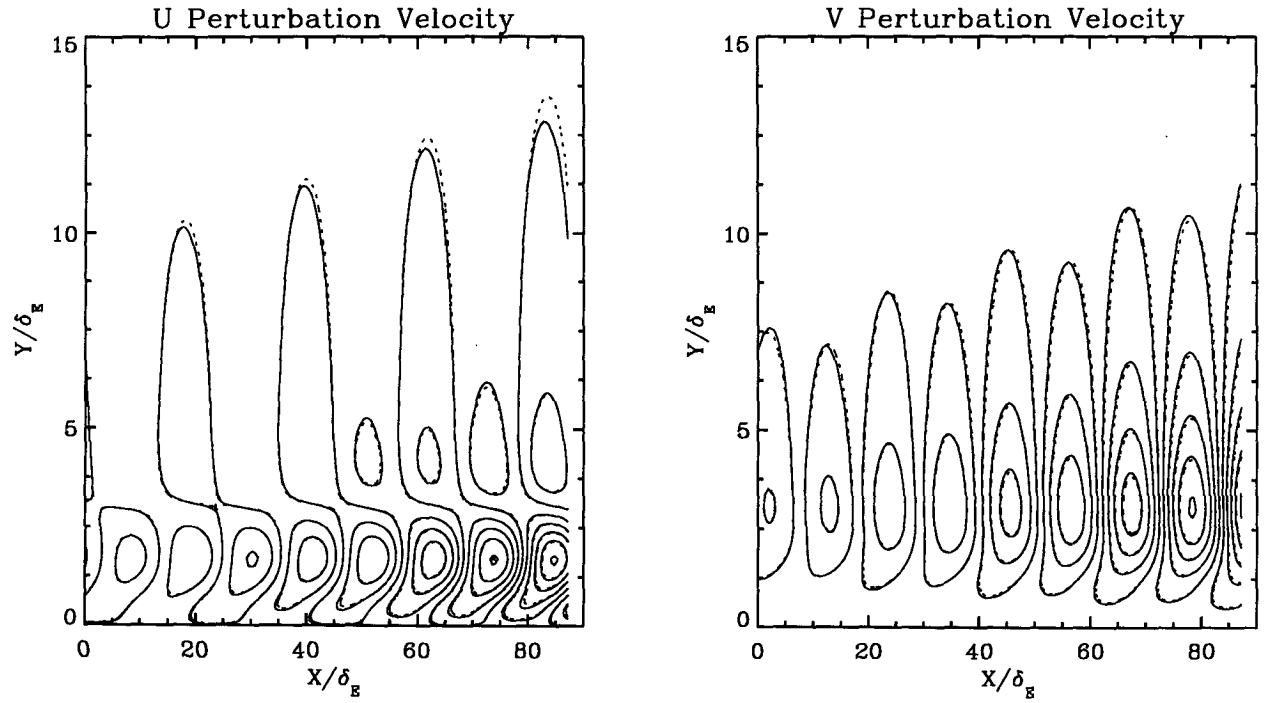

FIG. 2. Perturbation velocity contours at Re = 65 from direct numerical simulation results (solid lines) and from spatial linear stability solutions (dotted lines). Contours of (a) u and (b) v perturbation velocities. Contours for w show similar agreement with linear theory.

plied to the Ekman-layer Type II instability. Linear results were compared with results from a direct simulation, confirming the applicability of Gaster relations to the Ekman-layer stability problem.

In both of the cases examined, the least stable spatial mode is more closely aligned with the geostrophic free stream than is the temporal mode. In Fig. 1b, the least stable spatial mode is nearly parallel to the geostrophic wind vector, while the temporal mode is oriented approximately 15° clockwise. This shift in orientation may explain the discrepancies between the experimentally observed Type II waves and the results of temporal linear theory.

This is interesting from an atmospheric perspective, given that the longitudinal vortices observed in the atmosphere also tend to be more closely aligned with the geostrophic wind direction (Brown 1980). Whether persistence of transitional structures into higher Reynolds number flows plays a role in large-scale lineal structures in the atmosphere remains an open question; results presented here indicate that attempts to answer this question might benefit by considering the spatial evolution of such structures.

Acknowledgments. This work was done under an Advanced Study Program Fellowship, under the auspices of the University Corporation for Atmospheric Research. The authors would like to thank Dr. Gökhan Danabasoglu at NCAR for providing us his Navier–Stokes solver, and Dr. James McWilliams, also at NCAR, for his helpful suggestions. We also thank the reviewers for their constructive comments. All computations were carried out using the NCAR Cray Y-MP.

REFERENCES

Brown, R. A., 1980: Longitudinal instabilities and secondary flows in the planetary boundary layer: A review. *Rev. Geophys. Space Phys.*, **18,** 683–697.

Caldwell, D. R., and C. W. Van Atta, 1970: Characteristics of Ekman boundary layer instabilities. *J. Fluid Mech.*, **44,** 70–95.

Danabasoglu, G., and S. Biringen, 1990: A Chebyshev matrix method for the spatial modes of the Orr–Sommerfeld equation. *J. Num. Meth. Fluids,* **11,** 1033–1037.

——, ——, and C. L. Streett, 1991: Spatial simulation of instability by periodic suction blowing. *Phys. Fluids A,* **13,** 2138–2147.

Etling, D., and R. A. Brown, 1993: Roll vortices in the planetary boundary layer: A review. *Bound.-Layer Meteor.*, **65,** 215–248.

Faller, A. J., 1965: Large eddies in the atmospheric boundary layer and their possible role in the formation of cloud rolls. *J. Atmos. Sci.*, **22,** 176–184.

——, 1990: Instability and transition of disturbed flow on a rotating disk. *J. Fluid Mech.*, **230,** 245–269.

——, and R. E. Kaylor, 1966: A numerical study of the instability of the laminar Ekman boundary layer. *J. Atmos. Sci.*, **23,** 466–480.

Gaster, M., 1962: A note on the relation between temporally increasing and spatially increasing disturbances in hydrodynamic stability. *J. Fluid Mech.*, **14,** 222–224.

Lilly, D. K., 1966: On the instability of the Ekman boundary layer. *J. Atmos. Sci.*, **23,** 481–493.

Marlatt, S. W., and S. Biringen, 1994: Numerical simulation of spatially evolving Ekman layer instability. *Phys. Fluids,* submitted.

Melander, M. V., 1983: An algorithmic approach to the linear stability of the Ekman layer. *J. Fluid Mech.*, **132,** 283–293.

Shirer, H. N., 1986: Cloud streets during KonTur: A comparison of parallel/thermal instability modes with observations. *Beitr. Phys. Atmos.*, **59,** 150–161.

Stensrud, D. J., and H. N. Shirer, 1988: Development of boundary layer rolls from dynamic instabilities. *J. Atmos. Sci.*, **45,** 1007–1019.

Tatro, P. R., and E. L. Mollo-Christensen, 1967: Experiments on Ekman layer stability. *J. Fluid Mech.*, **28,** 531–543.

Van Dooren, P., 1982: *Assoc. Comput. Mach. Trans. Math. Soft.*, **8,** 376–382.